

NGC 5694: another foster son of the Galactic Halo ^{*}

A. Mucciarelli,¹ M. Bellazzini,² M. Catelan,^{3,4} E. Dalessandro,¹ P. Amigo,^{3,4,5}
M. Correnti,⁶ C. Cortés,⁷ V. D’Orazi^{8,9}

¹ *Dipartimento di Fisica & Astronomia, Università degli Studi di Bologna, Viale Bertini Pichat, 6/2 - 40127, Bologna, Italy*

² *INAF-Osservatorio Astronomico di Bologna, Via Ranzani, 1 - 40127, Bologna, Italy*

³ *Pontificia Universidad Católica de Chile, Facultad de Física, Departamento de Astronomía y Astrofísica, Av. Vicuña Mackenna 4860, 782-0436 Macul, Santiago, Chile*

⁴ *The Milky Way Millennium Nucleus, Av. Vicuña Mackenna 4860, 782-0436 Macul, Santiago, Chile*

⁵ *Departamento de Física y Astronomía, Universidad de Valparaíso, Av. Gran Bretaña 1111, Playa Ancha, Valparaíso, Chile*

⁶ *INAF-Istituto di Astrofisica Spaziale e Fisica Cosmica, Via Gobetti 101, I-40129, Bologna, Italy*

⁷ *Departamento de Física, Facultad de Ciencias Básicas, Universidad Metropolitana de Ciencias de la Educación, Av. José Pedro Alessandri 774, 776-0197 Ñuñoa, Santiago, Chile*

⁸ *Department of Physics and Astronomy, Macquarie University, Balaclava Rd, North Ryde, NSW2109, Australia*

⁹ *Monash Centre for Astrophysics, School of Mathematical Sciences, Building 28, Monash University, VIC3800, Australia*

31 August 2021

ABSTRACT

We present the results of the analysis of high-resolution spectra obtained with UVES-FLAMES@VLT for six red giant branch stars in the outer-halo metal-poor ($[\text{Fe}/\text{H}]_{\text{I}} = -1.98$ and $[\text{Fe}/\text{H}]_{\text{II}} = -1.83$) Galactic globular cluster NGC 5694, which has been suggested as a possible incomer by Lee et al. (2006) based on the anomalous chemical composition of a single cluster giant. We obtain accurate abundances for a large number of elements and we find that: (a) the six target stars have the same chemical composition within the uncertainties, except for Na and Al; (b) the average cluster abundance of α elements (with the only exception of Si) is nearly solar, at odds with typical halo stars and globular clusters of similar metallicity; (c) Y, Ba, La and Eu abundances are also significantly lower than in Galactic field stars and star clusters of similar metallicity. Hence we confirm the Lee et al. classification of NGC 5694 as a cluster of extra-galactic origin. We provide the first insight on the Na-O and Mg-Al anti-correlations in this cluster: all the considered stars have very similar abundance ratios for these elements, except one that has significantly lower $[\text{Na}/\text{Fe}]$ and $[\text{Al}/\text{Fe}]$ ratios, suggesting that some degree of early self-enrichment has occurred also in this cluster.

Key words: stars: abundances — globular clusters: individual: NGC 5694 — techniques: spectroscopic

1 INTRODUCTION

Modern wide-area optical surveys have revealed that the stellar halo of nearby galaxies (including our own) contains a wealth of substructures due to the accretion of smaller haloes (see, e.g., Ibata et al. 2007; Bell et al. 2008, and references therein), as expected in a hierarchical merging scenario for galaxy formation (e.g., Bullock & Johnston 2005; Abadi et al. 2006, and references therein). It is now observationally established that the accretion of satellites leads also to the accretion of their globular clusters (GC;

Bellazzini et al. 2003; Law & Majewski 2010; Mackey et al. 2010, 2013). Therefore, searching for Galactic GCs that can be identified as coming from disrupted satellites is one possible research lines to investigate the assembly history of the Milky Way halo and the associated GC system.

A powerful technique to spot individual members of an ancient accretion event (either a star or a star cluster) consists in finding some peculiar feature in their elemental abundance pattern markedly different from typical Halo stars, the so-called *chemical tagging* (see Freeman & Bland-Hawthorn 2002; Schlafman et al. 2012; Mitschang et al. 2013, for recent applications, discussion and references). Examples of the identification of likely accreted GCs by means of chem-

^{*} Based on data obtained at the Very Large Telescope under the programs 073.D-0211 and 089.D-0094.

ical tagging are provided by Cohen (2004) for Palomar 12, and by Mottini et al. (2008) for Ruprecht 106.

In this framework, Lee et al. (2006, L06 hereafter) obtained high-resolution spectroscopy of a bright red giant branch (RGB) star in the Galactic cluster NGC 5694, already indicated as a possible incomer by Harris & Hesser (1976) because of its large distance and velocity ($R_{GC} \simeq 30$ kpc, $V_r \simeq -140$ km/s; Correnti et al. 2011; Geisler et al. 1995). Intriguingly, Correnti et al. (2011) found that the cluster density profile is much more extended than previously believed and declines, in the outer fringes of the cluster, with a slope that is not reproduced by model profiles generally adopted for classical GCs. L06 derived the chemical abundance for several elements in the considered star and revealed that it displays $[\alpha/\text{Fe}]$, $[\text{Ba}/\text{Fe}]$ and (possibly) $[\text{Cu}/\text{Fe}]$ ratios significantly different from those of typical halo stars and of the bulk of Galactic GCs of similar metallicity, concluding that the cluster has an extra-galactic origin. This conclusion is clearly very interesting, but it is based on a single cluster star, virtually located at the very tip of the RGB.

To obtain a clear-cut confirmation of the tagging of NGC 5694 proposed by L06 we obtained high-resolution spectra of *six* cluster members. In this paper we present the results of the analysis of these spectra. We obtained elemental abundances that fully confirm (and extend) the results by L06. In addition, we provide the first insight into the early self-enrichment history of this cluster, as traced by the spread in Na, O, Mg, and Al, that has been recently recognized as a common feature of old GCs (see Gratton et al. 2012, and references therein).

2 OBSERVATIONS

The data have been acquired with the FLAMES@VLT spectrograph in the combined MEDUSA+UVES mode, allowing the simultaneous allocation of 8 UVES high-resolution fibers (discussed in this paper) and 132 MEDUSA mid-resolution fibers (discussed in a forthcoming paper, mainly devoted to the internal kinematics of the cluster). The employed spectral configuration for the UVES targets discussed in this paper is the 580 Red Arm, with a spectral resolution of ~ 40000 and covering the range $\sim 4800\text{--}6800 \text{ \AA}$. A total of 8 exposures of 46 min each for the same targets configuration has been secured in Service Mode during the period between April and July 2012. The targets have been selected in the bright portion of the RGB ($V < 16.5$) from the B,V photometric catalog by Correnti et al. (2011, C11 hereafter; from VIMOS@VLT observations over a $24' \times 20'$ field of view), complemented with publicly available WFPC2@HST photometry of the central region from Piotto et al. (2002). We selected our UVES targets among stars already confirmed as cluster members from their radial velocity by Geisler et al. (1995); among them, we included also the only star analyzed by L06, namely our star #37. To avoid significant contamination from other sources, we excluded from the original target list any star (of magnitude V_0) having a companion with $V < V_0 + 1.0$ within two arcsec of its center. Two out of the eight available UVES fibers have been used to sample the sky background and perform a robust sky subtraction for each individual exposure. The position of the six tar-

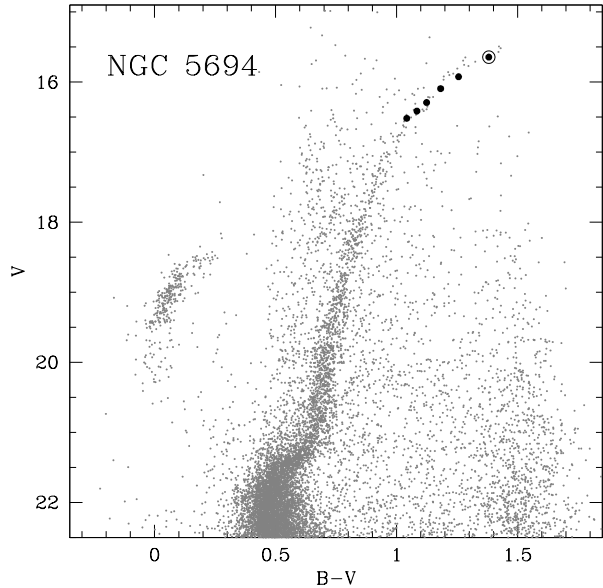


Figure 1. CMD of NGC 5694: the stars analyzed in this paper are highlighted as filled circles (the empty circle marks the star #37, in common with L06).

get stars in the cluster Color Magnitude Diagram (CMD) is shown in Fig.1, and their basic parameters are reported in Table 1.

The data reduction has been performed using the last version of the FLAMES-UVES CPL-based ESO pipeline¹, including bias-subtraction, flat-fielding, wavelength calibration with a standard Th-Ar lamp and spectral extraction. The dispersion solution has been checked by measuring the position of several sky emission lines and comparing them with their rest-frame position taken from the sky lines atlas by Osterbrock et al. (1996), finding no relevant wavelength shifts. We found that the final merged spectra obtained from the ESO pipeline are not satisfactory because of the quite poor quality in the overlapping region of adjacent orders. Thus, we decided to perform the order merging under IRAF.

Each single (sky-subtracted) exposure of a given star has been converted to the heliocentric system (the heliocentric correction has been computed with the IRAF task *rvcorrect*) and finally coadded together in order to obtain a median spectrum (thus removing spikes, cosmic rays and other random spectral impurities). The typical SNR per pixel for the brightest star are ~ 60 at $\sim 5300 \text{ \AA}$ and ~ 80 at $\sim 6300 \text{ \AA}$; for the faintest star the SNR are ~ 30 and ~ 50 , at ~ 5300 and $\sim 6300 \text{ \AA}$, respectively.

2.1 Radial velocities

Radial velocities (RV) have been derived using the DAOSPEC code (Stetson & Pancino 2008), through the identification of $\sim 250\text{--}300$ absorption lines in each star. The two UVES chips are analyzed independently; the agreement between the two radial velocity estimates is excellent

¹ <http://www.eso.org/sci/software/pipelines/>

($\langle RV^{lower}-RV^{upper} \rangle = -0.28$ km/s, $\sigma = 0.24$ km/s). The typical uncertainty arising from this procedure (internal error) is ~ 0.05 km/s, but the dominant source of uncertainty is the zero-point of the wavelength calibration that we estimated by measuring the position of several emission and absorption telluric features. The uncertainty in the wavelength calibration (typically 0.3-0.5 km/s) is added in quadrature to the internal error. The heliocentric RV and total uncertainty for each target star are listed in Table 1.

The average RV is $V_r = -140.4 \pm 2.2$ km/s ($\sigma = 5.4$ km/s). This value nicely agrees with those derived by Geisler et al. (1995) and L06. The mean difference between our RV and those listed by Geisler et al. (1995) is of $\langle RV_{\text{this work}} - RV_{\text{Geisler et al. (1995)}} \rangle = +0.6$ km/s, with a dispersion of $\sigma = 6.9$ km/s, that can be considered as satisfying given the low-resolution of the spectra analyzed by Geisler et al. (1995, $R \approx 3000$). Also, we find an excellent agreement ($\langle RV_{\text{this work}} - RV_{\text{L06}} \rangle = +0.0$ km/s) with the RV value provided by L06 for the star #37, by using spectra with a spectral resolution similar to that of UVES.

3 CHEMICAL ANALYSIS

The determination of the chemical abundances for the majority of the elements has been obtained through the measurement of the equivalent widths (EWs) of atomic transition lines and employing the package GALA (Mucciarelli et al. 2013) based on the WIDTH9 code by R. L. Kurucz. For the lines that cannot be treated with the EWs method (because they are blended with other lines) we resort to the comparison between the observed and synthetic spectra. Model atmospheres have been computed with the last version of the ATLAS9 code, assuming local thermodynamic equilibrium (LTE) for all the species and one-dimensional, plane-parallel geometry. In the flux computation we cannot take into account the *approximate* overshooting (Castelli et al. 1997). The opacity distribution functions employed in the model calculations are those available in the website of F.Castelli² computed for a metallicity $[M/H] = -2.0$ dex (according to L06) and with solar-scaled abundance patterns for each element of the chemical mixture.

All the chemical abundances have been derived under the assumption of LTE. Corrections for departures from the LTE approximation are applied only for the Na lines, by interpolating on the grid of corrections calculated by Lind et al. (2011a). The grid by Lind et al. (2011a) does not include the cases with $\log g < 1$, while three program stars have surface gravity slightly lower than this boundary. For these stars the corrections have been computed assuming $\log g = 1$. Since the corrections are small and only weakly dependent on stellar parameters - in the considered range - this approximation should have a negligible impact on the final abundance estimates.

Reference solar abundances are from Grevesse & Sauval et al. (1998) except for oxygen, for which we adopted the most recent value by Caffau et al. (2008).

3.1 Atmospheric parameters

Due to the combination of low metallicity and low surface gravity of our targets, a fully spectroscopic derivation of all the atmospheric parameters could be biased from departures from LTE conditions (as discussed in Section 3.2). In order to avoid this kind of problems, we resort to photometry to derive effective temperatures (T_{eff}) and surface gravities ($\log g$). Atmospheric parameters have been derived from B,V photometry in the C11 catalog (with the expansion described in Sect. 2).

T_{eff} values have been computed by means of the $(B - V)_0 - T_{eff}$ transformation by Alonso et al. (1999) based on the Infrared Flux Method; the dereddened color $(B - V)_0$ is obtained adopting a color excess $E(B-V) = 0.099$ mag (C11) and the extinction law by McCall (2004). Surface gravities have been computed with the Stefan-Boltzmann relation, assuming the photometric T_{eff} , the distance modulus of 17.75 ± 0.10 (C11) and an evolutionary mass of $0.75 M_\odot$, as estimated from the isochrone from the BaSTI dataset (Pietrinferni et al. 2004) with age of 12 Gyr, $Z = 0.0003$ and a solar-scaled chemical mixture (according to L06)³. The bolometric corrections are calculated according to Eq. (17) of Alonso et al. (1999). Microturbulent velocities (v_t) have been estimated by minimizing the slope between the neutral iron lines and their reduced EWs (obtained as the logarithm of the EW normalized to its wavelength).

Uncertainties in T_{eff} are estimated by taking into account the uncertainty in B and V magnitudes and in the color excess. For the very bright stars considered here, the dominant factor in the photometric error is the uncertainty in photometric zero-point: here we conservatively assume a photometric error of 0.03 mag in both filters for all the targets. For the color excess $E(B-V)$ we adopted an uncertainty of 0.02 mag. The total uncertainty (photometry + extinction) corresponds to a typical uncertainty in T_{eff} of ~ 50 -60 K.

Uncertainties in the surface gravity are derived by considering the error sources in T_{eff} , luminosity (including the uncertainties of the photometry and in the distance modulus) and in mass (that we assume $= \pm 0.05 M_\odot$, corresponding to the typical spread in total mass along the horizontal branch of globular clusters, see e.g. Valcarce & Catelan (2008)). Summing all these terms in quadrature leads to a typical uncertainty in $\log g$ of 0.06 dex.

Finally, the error associated to the determination of v_t is estimated by propagating the uncertainty in the slope in the reduced EW vs Fe abundance plane, through a Jackknife bootstrap technique (Lupton 1993). This uncertainty is as small as ~ 0.08 km/s, thanks to the large number of Fe I lines used to determine v_t . To this value we added in quadrature the uncertainty in v_t due to the covariance with the other parameters: T_{eff} has been varied by $\pm 1\sigma_{T_{eff}}$ (thus leading to a variation of $\log g$) and the procedure to derive v_t has been repeated. Finally, we estimated a typical error in v_t of ± 0.15 km/s.

³ The choice of the stellar mass is affected by the details of the mass loss, a process not easy to model and still poorly known. However, the adoption of different values of the stellar mass has a very small (< 0.02 -0.03 dex) impact on the derived abundances.

² <http://wwwuser.oat.ts.astro.it/castelli/odfnew.html>

3.2 A comment about LTE and NLTE

Late-type stars with low metallicities and surface gravities (i.e. approaching the RGB-Tip) are expected to suffer from deviations from LTE conditions due to the occurrence of over-ionization because of the UV radiation excess (basically $J_\nu > B_\nu$, where J_ν is the source function and B_ν is the Planck function, see e.g. Asplund 2005).

The occurrence of these NLTE effects thwarts the derivation of $\log g$ from the ionization equilibrium, i.e. from the requirement that Fe I and Fe II are the same within the uncertainties. Basically, a forced ionization equilibrium in over-ionization conditions leads to underestimate the surface gravities. For our targets we found, on average, that $\langle \text{Fe I} - \text{Fe II} \rangle = -0.13$ dex ($\sigma = 0.05$ dex). To erase this offset we need to adopt lower $\log g$ values, typically between 0.0 and 0.3, incompatible with the stellar evolution predictions for a low-mass star in the bright portion of the RGB, in an old and metal-poor stellar system as NGC 5694. For instance, the isochrone used to derive the gravities predicts a surface gravity of 0.47 for its brightest point. Note that a fully spectroscopic analysis leads to temperatures lower by ~ 100 K than those predicted from the isochrone. Also, we checked that this offset cannot be a spurious effect due to the adopted $\log g$ values: an analysis performed on the solar flux spectrum of Neckel & Labs (1984), adopting the solar ATLAS9 model atmosphere computed by F. Castelli⁴, provides Fe I-Fe II = -0.01 ± 0.02 dex, excluding systematic offsets between the oscillator strengths of Fe I and Fe II lines. Thus, we can easily attribute the discrepancy between Fe I and Fe II abundances in the stars of NGC 5694 to NLTE effects.

In order to reduce the effects due to over-ionization, we decide to calculate the abundance ratios from neutral lines by scaling the abundance on the Fe I abundance and those from single ionized lines by scaling the abundance on Fe II. In fact, lines of the same ionization stage have similar dependencies from the parameter (in particular from the gravity). Among the elements derived from neutral lines, only the [O/Fe] abundance ratio has been scaled on Fe II, because the over-ionization effects are reduced from its first ionization potential and the oxygen abundance (when derived from the forbidden O line at 6300.3 Å, as we have done) has a sensitivity to the gravity similar to that of the ionized elements (we refer the reader to the detailed discussion in Ivans et al. 2001).

3.3 Line list

We selected the transitions to be analyzed through the visual inspection of synthetic spectra calculated with the atmospheric parameters of the targets (and assuming a global metallicity $[M/H] = -2.0$ dex, with solar-scaled abundance ratios for all the elements) and convolved with a Gaussian profile at the UVES resolution. The selected lines are chosen unblended from other transitions. Oscillator strengths and excitational potential are taken from the last version of the Kurucz/Castelli line-list⁵. When available, the Van

der Waals damping constants for the broadening by neutral hydrogen collisions calculated by Barklem et al. (2000) have been adopted, and for the other transitions we adopted the values from the Kurucz database or, when the Van der Waals constants are not available in the literature, they are computed by adopting the approximate formulas discussed in Castelli (2005). After a first analysis, we refine the line-list repeating the procedure of the lines selection by using synthetic spectra computed with the proper chemical composition of each star; typically, only a few lines are discarded at this step because they are blended with other transitions, and a few new transitions added to the line-list. Finally, the analysis is repeated with the clean line-list.

3.4 Abundances from equivalent widths

EWs have been measured with the code DAOSPEC (Stetson & Pancino 2008) that automatically performs the line profile fitting adopting a saturated Gaussian function, defined as $h(\lambda) = \frac{g(\lambda)}{1+g(\lambda)}$, where $g(\lambda)$ is the value of the Gaussian function at a given wavelength λ . All the spectral lines are fitted by adopting a fixed Full Width at Half Maximum (FWHM), that scales with the wavelength, as in wavelength-calibrated echelle spectra the spectral resolution remains constant along the entire spectrum and the FWHM varies with λ .

The FWHM for each spectrum has been estimated iteratively: we performed a first analysis using as input value the nominal FWHM of the grating, leaving DAOSPEC free to re-adjust the FWHM in order to minimize the median value of the residuals distribution. The new value of the FWHM (referred to the center of the spectrum) is used as input value for a new run, until a convergence of ~ 0.1 pixel is reached. After a visual inspection of the spectra and the check of the final residuals, we adopted for the normalization a 3rd-order Legendre polynomial. We checked that the use of a slightly different degree changes the derived FWHM at a level of 0.1-0.2 pixels, with a negligible impact on the EWs.

We include in the chemical analysis only lines that satisfy the following criteria:

- EW error smaller than 20%. As EW uncertainty we assumed the error estimated by DAOSPEC from the standard deviation of the local flux residuals and representing a 68% confidence interval of the derived EW. An error in EW of $\pm 20\%$ translates into an abundance error of ± 0.1 dex for a line located in the linear part of the curve of growth (typically, the lines with EW errors larger than $\sim 10\%$ are the weakest ones). The median abundance error due to the EW uncertainty for our lines is of ± 0.05 dex (only a few lines have abundance errors larger than 0.1 dex);

- a reduced EW smaller than -4.7 , corresponding to ~ 100 mÅ for a line at 5300 Å and ~ 120 mÅ for a line at 6300 Å. This boundary allows to exclude lines in the flat part of the curve of growth, that are less sensitive to the abundance, highly sensitive to the microturbulent velocity and the velocity fields, and for which the Gaussian approximation starts to fail, because of the development of Lorentzian wings in the line profile;

- a reduced EW larger than -6 , corresponding to ~ 5 and

⁴ <http://wwwuser.oat.ts.astro.it/castelli/sun/ap00t5777g44377k1odfnewings>

⁵ <http://wwwuser.oat.ts.astro.it/castelli/line-lists.html>

~ 6 mÅ at 5300 and 6300 Å, respectively. This boundary excludes lines that are too weak and noisy;

- DAOSPEC quality parameter Q lower than 1.2 in all the spectra. This parameter is the ratio between the local intensity residual of a given line and the root-mean-square intensity residual of the entire spectrum. Typically, only a couple of lines have been discarded because their Q parameters are systematically higher than the adopted threshold in each spectrum.

At the end of the analysis, the mean abundance (and the corresponding dispersion) for a given element in a given star is computed by averaging the abundances of the surviving lines weighted by the uncertainty on the abundance as obtained from the EW error. For those element for which only one line is available, the error associated to the individual abundance estimate is taken as the internal error.

Table 2 lists some measured EWs and atomic data, the complete set being available in the online journal.

3.5 Abundances from spectral synthesis

We compare the observed spectra with synthetic spectra to derive the abundance from those lines that exhibit a composite line structure. The oxygen abundance has been derived from the forbidden line at 6300.31 Å⁶, including the contribution of a close Ni line (for each star we adopted the corresponding Ni abundance derived from EWs). Odd-Z, iron-peak elements (Sc II, V I, Mn I, Co I and Cu I) suffer from hyperfine splitting and we adopted for those transitions the line-list provided in the Kurucz database⁷. For Cu the only available transition is that at 5105 Å, because the other Cu line usually investigated (at 5782 Å) falls in the gap between the two UVES chips. For Ba II we measured the red lines at 5853.7, 6141.7 and 6496.9 Å using the line-list available in the NIST database taking into account both hyperfine structure and isotopic splitting. Other Ba II lines are available in the blue part of our spectra but we excluded these transitions because they can be affected by relevant NLTE effects (see Sneden et al. 1996). We derived only 3σ detection upper limits for the strongest La II and Eu II available lines, at 6390.5 and 6645.1 Å, respectively. Also for these two lines, the modeling of synthetic spectra includes the hyperfine structure and (only for Eu II) isotopic splitting, by using the line-list by Lawler et al. (2001a) and Lawler et al. (2001b) for La and Eu, respectively.

The abundance for each selected line has been derived through a χ^2 -minimization between the observed spectrum and a grid of synthetic spectra calculated at different abundances. The synthetic spectra have been computed by means of SYNTH code developed by R. L. Kurucz, including the entire Kurucz/Castelli line-list (both for atomic and molecular transitions) and adopting the same model atmospheres used to derive the abundances from EWs. The synthetic spectra are convolved at the instrumental resolution, then rebinned at the same pixel-step of the observed

⁶ This transition is often superimposed on telluric lines both in absorption and emission; we carefully checked that in all the targets the oxygen line is not contaminated by telluric features.

⁷ <http://kurucz.harvard.edu/line-lists/gfhyper100/>

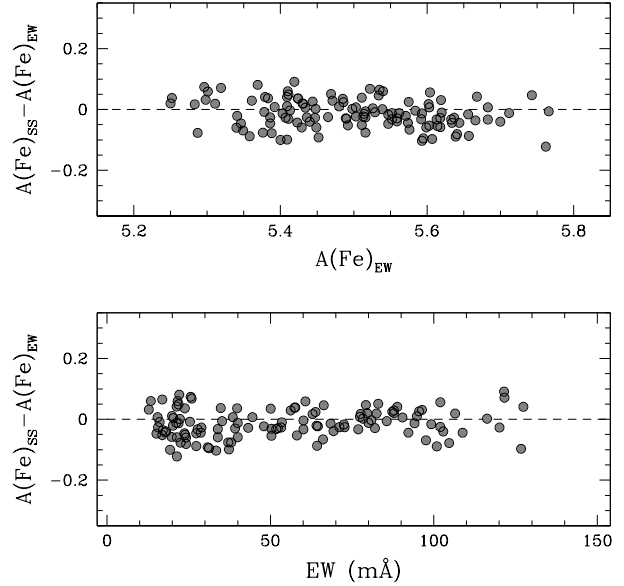


Figure 2. Difference of the abundances of neutral iron lines for the star #37 as inferred from spectral synthesis and EW measurements as a function of the iron abundance (from EWs, upper panel) and of the EW (lower panel). Horizontal dashed lines mark the zero value.

spectra (0.014 and 0.017 Å/pixel for the lower and upper chip of the 580 Red Arm grating, respectively). Additional details about the fitting procedure are discussed in Mucciarelli et al. (2012b).

The uncertainty in the line fitting procedure has been estimated by means of Monte Carlo simulations: for each line the fitting procedure has been repeated by using a sample of 500 synthetic spectra where Poissonian noise has been injected (after the re-mapping of the synthetic spectra at the same pixel-step of the UVES spectra) in order to reproduce the noise conditions observed around the analysed line. These uncertainties (ranging from ~ 0.02 dex up to ~ 0.07 dex, for SNR= 70 and 30, respectively for a line of moderate strength) have been used as weights to compute the average abundance for a given species or as internal error when only one line is available, as done for abundance estimates derived from EWs.

In order to check possible systematic offsets between the abundances inferred with the two methodologies (EWs and spectral synthesis) we re-analysed with the method described above the Fe I lines for the star #37 (taken as representative of our sample). Fig. 2 shows the difference between the $A(\text{Fe I})$ abundances inferred with the two methods as a function of the iron abundances derived from EWs (upper panel) and of the EWs (lower panel). The average difference turns out to be $A(\text{Fe I})_{SS} - A(\text{Fe I})_{EW} = -0.013$ dex ($\sigma = 0.047$ dex); also, none specific behaviour with the line strength is found. This check confirms that the two methods provide basically the same results.

3.6 Abundance uncertainties

The total uncertainty for a given elemental abundance is computed as the sum in quadrature of two sources of error: (1) that arising from the measurement procedure (EW or spectral synthesis), and (2) that arising from the atmospheric parameters. The measurement errors are computed as described in Sections 3.4 and 3.5.

Internal uncertainties related to the measurement errors for each elemental abundance are computed as the dispersion of the mean normalized to the root mean square of the number of used lines. Uncertainties due to atmospheric parameters are calculated by varying each time only one parameter by the corresponding error, keeping the other ones fixed and repeating the analysis.

As discussed by several authors (see e.g. McWilliam et al. 2005; Barklem et al. 2005), when we obtain the abundance ratios (as $[X/Y]=[X/H]-[Y/H]$) the systematic uncertainties related to the atmospheric parameters partially cancel out, because, in general, lines of the same ionization stage respond in a similar way to changes in the stellar parameters. For instance, the estimated abundance variation due to $\pm 1\sigma_{T_{eff}}$ for the star #37 is of $^{+0.07}_{-0.06}$ for Fe and of $^{+0.07}_{-0.07}$ for Ca. Therefore, an error in T_{eff} of that amplitude translates into variations of the two considered quantities amounting to just $^{+0.00}_{-0.01}$ in the corresponding $[Ca/Fe]$ abundance ratio. On the other hand, the internal errors due to the (EWs or spectral synthesis) measurements are independent and they will be combined in quadrature for each abundance ratio. Thus, we provide for each element two different estimates of the total uncertainty: (1) the uncertainty for the absolute abundance $[X/H]$ obtained by combining in quadrature the internal error and those related to each atmospheric parameter, and (2) the uncertainty for the abundance ratio $[X/Fe]$ (where the reference iron abundance is that from Fe I lines for neutral elements and from Fe II lines for single ionized elements) obtained by summing in quadrature the internal errors of X and Fe, and the relative abundance variation due to each atmospheric parameter.

3.7 Results and comparison with L06

Table 3 summarizes the measured abundance ratios in the target stars, together with the adopted reference solar value and the total uncertainty. Reported errors are the total uncertainties of the $[X/Fe]$ abundance ratios, while the values in the brackets are the uncertainties of the $[X/H]$ abundance ratios (see Sect. 3.6).

The inclusion in our sample of the star studied by L06 (our star #37) give us the opportunity to check the reliability of our abundances by the comparison with a completely independent analysis, based on independent photometry and high-resolution spectra (from MIKE@MAGELLAN). The elemental abundances for Fe, Mg, Si, Ca, Ti, Mn, Ni, Cu, Y, Ba, La and Eu have been obtained in both studies, for this star.

The atmospheric parameters adopted in the two analyses are very similar ($\delta T_{eff}=20$ K, $\delta \log g=0.05$ and $\delta v_t=0.3$ km/s). We find small differences in the iron content, with $Fe_{us} - Fe_{Lee06}=+0.07$ dex and $+0.10$ dex for neutral and single ionized Fe lines. Basically, these differences are fully

ascribable to the differences in the atmospheric parameters (mainly the difference in v_t). We re-analyse this star by adopting the same atmospheric parameters as in L06. Considering also the small offset in the employed solar iron abundance ($\delta Fe_{\odot}=0.02$), the difference turns out to be of $+0.02$ for $[Fe/H]$ I and 0.0 for $[Fe/H]$ II.

For the other abundance ratios, the typical offset are smaller than 0.1 dex, except for Mn ($[Mn/Fe]_{us} - [Mn/Fe]_{Lee06}=-0.22$ dex) and Ba ($[Ba/Fe]_{us} - [Ba/Fe]_{Lee06}=-0.24$ dex). However also these differences are within the combined uncertainties of the two estimates. At least for Ba, the offset can be easily ascribed to the different v_t values adopted in the two analyses, because the Ba II lines are located in the flat part of the curve of growth and they are sensitive to the velocity fields. Unfortunately, L06 do not provide details about the employed hyperfine structure, oscillator strength and isotopic splitting for the lines derived by spectral synthesis and we are thus unable to properly compare the corresponding abundances.

For La and Eu, the spectrum acquired by L06 has a higher SNR with respect to our one, thus they are able to properly measure the abundances for these elements, while we can provide only upper limits. However, our upper limits are consistent with their results.

It may be worth noting that star #37 has been recognized as a semi-regular variable by Rodrigues de Andrade et al. (2012, their V12). The V magnitude of the star in the 26 epochs sampled by these authors, spread over ~ 100 days, shows a typical r.m.s. scatter of a few hundredths of a magnitude (a maximum $\Delta V \lesssim 0.1$ mag). This suggests that the amplitude of the variation is so small as have negligible effect on the chemical abundance analysis, as confirmed also by the excellent agreement between our results and those by L06, derived from data obtained in different epochs and as described above.

3.8 Defining a test case for differential comparison: NGC 6397

Since the main scientific goal of the present study is to verify if NGC 5694 has indeed a chemical abundance pattern setting it apart from the bulk of classical Galactic GCs of similar metallicity, it seems safe to test the hypothesis against a bona-fide, *typical* MW halo cluster, by adopting a *strictly homogeneous analysis on very similar data*.

With this aim, we retrieved, from the ESO Archive⁸, the UVES@FLAMES red-arm spectra of 13 giant stars of the GC NGC 6397 (that has the same metallicity of NGC 5694 and an abundance pattern typical of the MW halo, see e.g. Carretta et al. 2009b; Lind et al. 2011b; Lovisi et al. 2012) taken with the same instrumental configuration used here for NGC 5694.

Atmospheric parameters have been determined with the same technique described in Section 4.1, adopting the B, V photometry used by Carretta et al. (2009b) and following the same steps of the analysis described above. Even if these giants of NGC 6397 are slightly less evolved with respect to

⁸ <http://archive.eso.org/cms/>

those of NGC 5694 (with T_{eff} in the range ~ 4700 - 4900 K and $\log g$ between 1.5 and 2.0), we analysed them with the line-list optimized for the targets of NGC 5694, to maintain the full homogeneity of the analysis. For this reason, some transitions detectable in our NGC 5694 stars cannot be measured in the stars of the NGC 6397 sample because they are too weak in their warmer atmospheres (in spite of the nearly identical metallicity of the two clusters). The derived average abundances for a number of elements are reported in Table 4 (together with the differences δ between the abundance ratios measured in NGC 5694 and NGC 6397) and will be discussed in the following, providing an extremely robust differential benchmark for the comparison with NGC 5694 (see Sect. 4.1 for further details on the content of this table).

Here we simply note that from our analysis, NGC 6397 has $[Fe/H]I = -2.00 \pm 0.02$ and $[Fe/H]II = -1.90 \pm 0.01$, in nice agreement with previous studies (Lind et al. 2011b; Koch & McWilliam 2011; Lovisi et al. 2012, and references therein). In particular, with respect to the analysis by Carretta et al. (2009a) based on the same spectra, we find an average difference $[Fe/H]I - [Fe/H]I_{Carretta09} = -0.01$ dex ($\sigma = 0.06$ dex) and $[Fe/H]II - [Fe/H]II_{Carretta09} = +0.13$ dex ($\sigma = 0.06$ dex), for neutral and ionized iron abundances, respectively.

The two clusters have very similar iron content, with a difference $[Fe/H]I_{NGC\ 5694} - [Fe/H]I_{NGC\ 6397} = +0.02$ dex and $[Fe/H]II_{NGC\ 5694} - [Fe/H]II_{NGC\ 6397} = +0.07$ dex, hence we can safely assume that they have indeed the same metallicity.

4 THE CHEMICAL COMPOSITION OF NGC 5694

4.1 Chemical homogeneity and iron abundance

As a first step in investigating the chemical properties of the cluster we check if the observed distributions of abundance ratios are consistent with chemical homogeneity, i.e. if all the stars have the same abundance of a given element within the uncertainties or if there is an *intrinsic* spread. To this aim we use the Maximum Likelihood (ML) algorithm described in Mucciarelli et al. (2012b), that provides the mean, the intrinsic spread (σ_{int}) and the respective uncertainties for a given set of abundances, properly taking into account individual observational errors, in the hypothesis that the considered distribution can be approximated by a Gaussian.

In Table 4 we summarize the mean value and the intrinsic spread of each abundance ratio, with the respective uncertainties as derived with the ML algorithm. Excluding Na and Al (discussed separately in Sect. 4.3), the target stars do not show significant spread in any of the derived abundance ratios. For $[Ni/Fe]$ we detected a formal non-null spread but fully consistent with zero, within the errors ($\sigma_{[Ni/Fe]} = +0.02 \pm 0.03$).

While the considered sample is too small to draw a firm conclusion concerning the cluster as a whole, these results strongly suggest that the stars in NGC 5694 are as chemical homogeneous as those of typical GCs (Carretta et al. 2009c). For this reason, in the following we will adopt the *average* cluster abundance, as reported in Table 4, instead

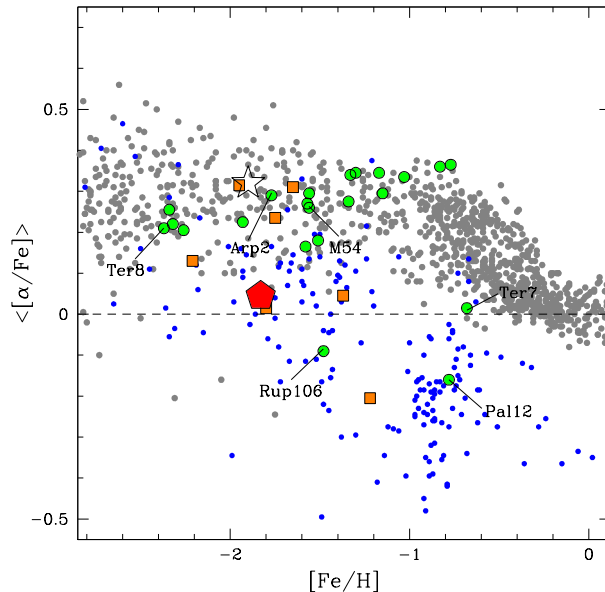


Figure 3. $\langle [\alpha/Fe] \rangle = 0.5(Ca+Ti)/Fe$ as a function of $[Fe/H]$ for different samples of stars and globular clusters. NGC 5694 is represented as a red filled pentagon, while the empty starred symbol indicates NGC 6397 (from our homogeneous analysis, see Section 3.8). Filled green circles are Galactic GCs; filled orange squares are old GCs of the LMC. Small grey filled circles are Galactic field stars; small blue circles are field stars in dSph satellites of the Milky Way. The dashed line marks the solar value of $\langle [\alpha/Fe] \rangle$.

of the abundances of individual stars for all the elements except Na and Al. This will make easier the comparison with other GCs.

For La and Eu we have only upper limits to the abundance, hence we do not provide intrinsic spreads and we assume as typical upper limits for the cluster the values of the upper limits derived for the star with the highest SNR.

The average iron content derived from the six giants analysed in this work is $[Fe/H]I = -1.98 \pm 0.03$ from neutral iron lines and $[Fe/H]II = -1.83 \pm 0.01$ from single ionized lines. As discussed in Sect. 3.2, the offset between the two iron abundances is likely due to over-ionization effects that can over-estimate the abundances derived from neutral lines. Thus, we rely on the $[Fe/H]$ ratio from single ionized lines as reliable estimate of the cluster metallicity.

4.2 Comparison with other stellar systems

In Fig.2–5 we compare the average abundance of NGC 5694 as derived in the present study (large filled pentagon) with several sets of stars and star clusters, for a few key abundance ratios. Our benchmark comparison cluster NGC 6397 (see Sect. 3.8, above) is represented as a large empty star.

The other data sources and symbols are the following:

- Galactic field stars (grey points) are from Edvardsson et al. (1993), Burris et al. (2000), Fulbright (2000), Stephens & Boesgaard (2002), Mishenina et al. (2002), Gratton et al. (2003), Reddy et al. (2003), Bihain et al. (2004), Barklem et al. (2005), Bensby et al. (2005), and Reddy et al. (2006).

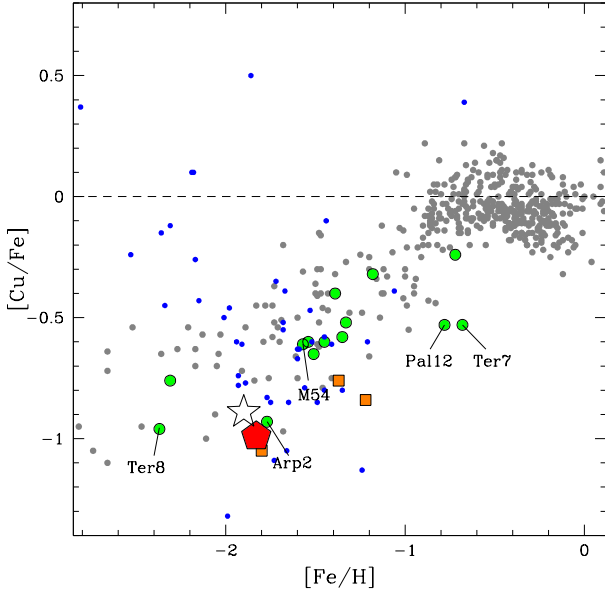


Figure 4. Behaviour of $[\text{Cu}/\text{Fe}]$ as a function of $[\text{Fe}/\text{H}]$. Same symbols of Fig. 3.

- Stars from dwarf spheroidal (dSph) galaxies (blue points) are from Shetrone et al. (2001, 2003, Carina, Fornax, Leo II, Sculptor, Ursa Minor and Sextans), Sbordone et al. (2007, Sagittarius), Koch et al. (2008, Carina), Cohen & Huang (2009, Draco), Letarte et al. (2010, Fornax), Frebel et al. (2010, Ursa Maior II and Coma Berenices), Venn et al. (2012, Carina) and Lemasle et al. (2012, Carina).

- Data for Galactic GCs (large green filled circles) for α -elements are from Carretta et al. (2009b), for Cu from Simmerer et al. (2003), for Ba from D’Orazi et al. (2010), for Eu from Sneden et al. (1997, 2004), Ivans et al. (1999, 2001), Ramirez & Cohen (2002), Lee & Carney (2002), James et al. (2004). GCs associated with the Sagittarius (Sgr) dSphs or with its tidal stream are labeled with their names: M 54 (Brown et al. 1999; Carretta et al. 2010), Arp 8 (Mottini et al. 2008), Palomar 12 (Cohen 2004), Terzan 7 (Sbordone et al. 2007) and Terzan 8 (Mottini et al. 2008). We did the same also for Ruprecht 106, strongly suspected as being of extra-galactic origin because of its lower-than-average age (Dotter et al. 2011) and peculiar abundance pattern (Brown et al. 1997)⁹.

- Old (age $\gtrsim 10$ Gyr) GCs in the Large Magellanic Cloud (LMC) are represented as filled orange squares. The data are from Johnson et al. (2006) and Mucciarelli et al. (2010).

4.2.1 Average abundances: α elements

The $[\alpha/\text{Fe}]$ ratios of NGC 5694 (see Tables 3 and 4) are around the solar value for O, Mg, Ca, and Ti, while only

⁹ Rup 106 was also tentatively associated with the so-called “Orphan Stream” by Fellhauer et al. (2007), but Newberg et al. (2010) rejected the association based on a more detailed determination of the orbit of the stream.

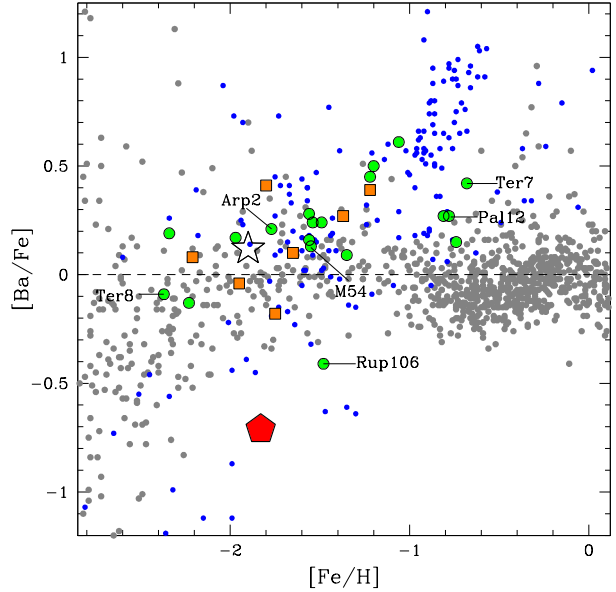


Figure 5. Behaviour of $[\text{Ba}/\text{Fe}]$ as a function of $[\text{Fe}/\text{H}]$. Same symbols of Fig. 3.

for Si the cluster shows an enhanced abundance ratio, more typical of Halo stars and clusters ($[\text{Si}/\text{Fe}] = +0.30 \pm 0.03$). In Fig. 2 we show the position of NGC 5694 in the $(\langle[\alpha/\text{Fe}]\rangle = [0.5(\text{Ca} + \text{Ti})/\text{Fe}]$ versus $[\text{Fe}/\text{H}]$ plane. The adopted combination of α elements is intended to be broadly representative of the group while (a) guaranteeing the largest sample of stars and GCs to compare with, since the abundances of these two elements are relatively easy to measure, and (b) being limited to elements that do not show significant abundance spread in ordinary GCs due to self-enrichment processes (like O and Mg; Gratton et al. 2012).

It is quite clear that the $[\alpha/\text{Fe}]$ ratio of NGC 5694 is significantly lower than any MW or LMC cluster having $[\text{Fe}/\text{H}] \leq -1.5$; moreover, it lies at the lower limit of the distribution of the bulk of Halo stars of similar metallicity. The direct – and strictly differential – comparison with NGC 6397 shows that, while the abundance of Si in the two clusters is not too different, Ca and Ti abundances in NGC 5694 are much (and very significantly) lower than in NGC 6397. O and Mg were not measured in our homogeneous analysis of this cluster (Sect. 3.8), but were obtained by Carretta et al. (2009b). They found significant intrinsic spread in the abundance of both elements and mean values of $[\text{O}/\text{Fe}] = +0.29$ and $[\text{Mg}/\text{Fe}] = +0.46$, both significantly larger than what we get for NGC 5694. Hence, we must conclude that the difference in the abundance pattern of α elements between NGC 5694 and classical Halo GCs is large, strongly significant and robustly established.

In Fig. 2, NGC 5694 appears to fall straight on the sequence defined by dSph stars, that is also populated by some Sgr and LMC clusters and by Rup 106. This clearly suggests an origin in the same kind of environment – a dwarf galaxy – also for NGC 5694.

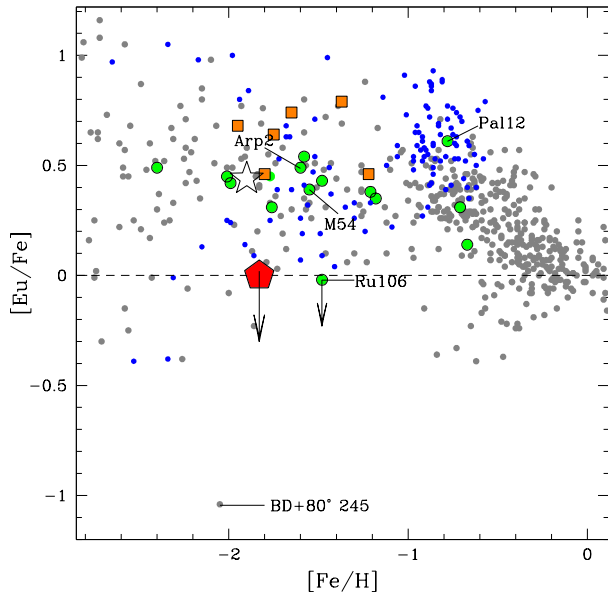


Figure 6. Behaviour of $[\text{Eu}/\text{Fe}]$ as a function of $[\text{Fe}/\text{H}]$. Same symbols of Fig. 3. Additionally, the position of the Galactic star $\text{BD}+80^\circ 245$ is shown (Carney et al. 1997).

4.2.2 Average abundances: iron-peak elements, copper, r- and s-elements

Iron-peak elements like Sc, V, Mn, Co and Cr have sub-solar abundance ratios, ranging from a mild depletion with respect to the solar value ($[\text{Cr}/\text{Fe}] = -0.14 \pm 0.02$ dex) to a significant depletion (as observed for Mn, with $[\text{Mn}/\text{Fe}] = -0.48 \pm 0.07$ dex). Among the iron-peak elements, only Ni has a solar-scaled abundance ratio ($[\text{Ni}/\text{Fe}] = -0.06 \pm 0.01$ dex). Differences between NGC 5694 and NGC 6397 of the order of ~ 0.25 dex (see Table 4) have been detected for $[\text{Sc}/\text{Fe}]$, $[\text{V}/\text{Fe}]$ and $[\text{Co}/\text{Fe}]$, while the $[\text{Mn}/\text{Fe}]$, $[\text{Cr}/\text{Fe}]$ and $[\text{Ni}/\text{Fe}]$ abundance ratios are compatible between the two clusters (with differences smaller than 0.1 dex).

NGC 5694 is remarkably deficient in Cu, $[\text{Cu}/\text{Fe}] = -0.99 \pm 0.06$, as noted also by L06. While the abundance of copper is at the lower limit of the Galactic halo stars distribution, it is pretty similar to that of NGC 6397, as well as to other metal-poor GCs (see Fig. 3).

An overall depletion of the slow neutron-capture elements is found, with $[\text{Y}/\text{Fe}]_{\text{II}} = -0.77 \pm 0.03$ and $[\text{Ba}/\text{Fe}]_{\text{II}} = -0.71 \pm 0.06$. The upper limits derived for $[\text{La}/\text{Fe}]_{\text{II}}$ and $[\text{Eu}/\text{Fe}]_{\text{II}}$ indicate sub-solar abundance ratios for both these elements. *The abundance ratios of Y, Ba, La, and Eu in NGC 5694 are significantly lower than in NGC 6397.* Fig. 4 shows at a first glance that the cluster has $[\text{Ba}/\text{Fe}]$ much lower than any other considered GC and than any Galactic field stars in the considered sample having $[\text{Fe}/\text{H}] \gtrsim -2.2$ (except one, see below)¹⁰. Only a couple of stars from the Carina dSph populates the same region of the diagram as NGC 5694, while the only other cluster showing a $[\text{Ba}/\text{Fe}]$

¹⁰ See Carney et al. (1997) for a small sample of Ba deficient Galactic stars in the solar neighborhood.

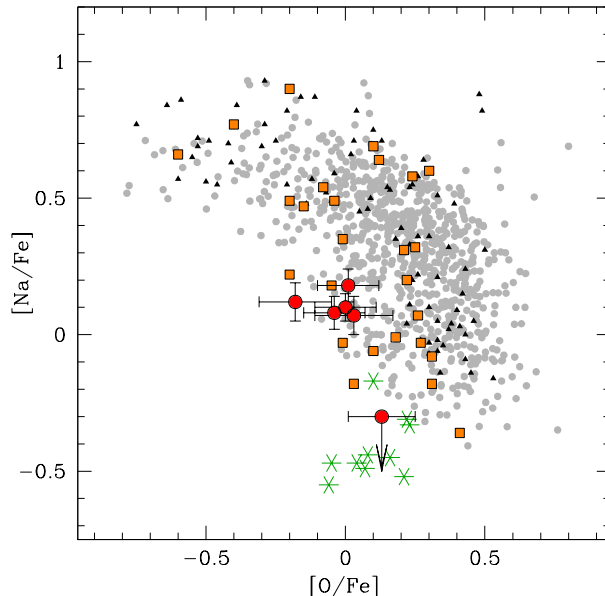


Figure 7. Behaviour of $[\text{Na}/\text{Fe}]$ as a function of $[\text{O}/\text{Fe}]$. Red circles are the individual stars of NGC 5694, in comparison with the individual stars in the Galactic GC sample by Carretta et al. (2009a, grey circles), in M54 (Carretta et al. 2010, black triangles), in the LMC old GCs (Johnson et al. 2006; Mucciarelli et al. 2010, orange squares) and in the GCs of extra-Galactic origin: Ruprecht 106, Palomar 12 and Terzan 7 (Brown et al. 1997; Cohen 2004; Sbordone et al. 2007, green asterisks).

ratio significantly lower than other GCs of similar metallicity is Rup 106.

The similarity between NGC 5694 and Rup 106 emerges also in the $[\text{Eu}/\text{Fe}]$ vs. $[\text{Fe}/\text{H}]$ plane, shown in Fig. 5. Both clusters stand out as remarkably Eu-deficient with respect to other GCs and both Galactic and dSph stars. In our "comparison sample" there is only one star that is strongly deficient in Eu, namely the solar-neighborhood sub-giant star $\text{BD}+80^\circ 245$, discovered by Carney et al. (1997), with $[\text{Fe}/\text{H}] = -2.05$ and $[\text{Eu}/\text{Fe}] = -1.04$ (Fulbright 2000). The star displays also sub-solar average $[\alpha/\text{Fe}]$ ratio and $[\text{Ba}/\text{Fe}] = -1.87$; given its peculiar abundance pattern and large apogalactic distance it has been indicated as having an extra-Galactic origin (Carney et al. 1997).

4.3 Elements displaying abundance spreads: Na, O, Mg, Al

An impressive amount of photometric and spectroscopic information collected in the past decade has reversed the classical paradigm of GCs as simple stellar populations, revealing the co-existence in the same cluster of different stellar generations with very small (less than ~ 200 Myr) age differences but distinct chemical abundance patterns (see Carretta et al. 2009a; Gratton et al. 2012, and references therein). As discussed by many authors (see e.g. Valcarce & Catelan 2011, and references therein), it is generally believed that the chemical enrichment of the GCs should have been driven by polluters like, e.g. AGB stars and/or fast rotating massive stars, ejecting into the intra-

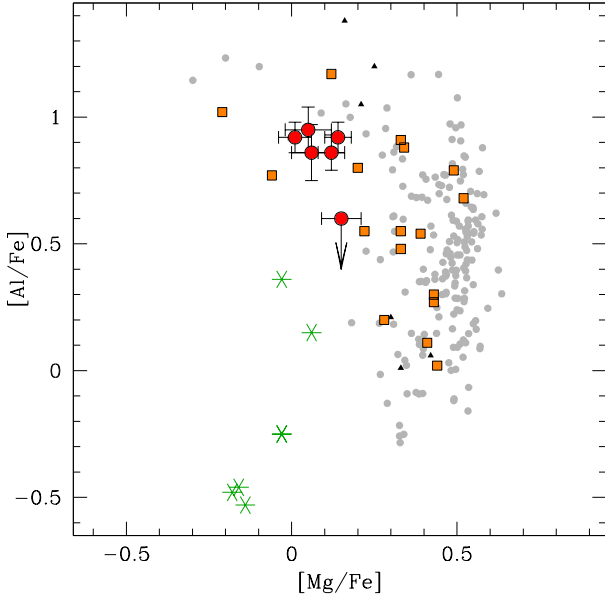


Figure 8. Behaviour of $[Mg/Fe]$ as a function of $[Al/Fe]$. Same symbols of Fig. 8.

cluster medium gas processed by CNO, Ne-Na and Mg-Al chains, leading to variations in light elements as He, C, N, Na, O, Mg and Al, without enrichment in iron and other heavy elements (driven by Supernovae explosions, whose ejecta cannot be retained in small mass systems as GCs). The Na-O (and, to a lesser extent, Mg-Al) anti-correlation is considered as a typical feature of all the old GCs massive enough to retain the gas of these low-energy pollutants in their early evolution and regardless of the parent galaxy (see Carretta et al. 2009b; Mucciarelli et al. 2010).

Figs. 7 and 8 show the position of the individual stars of NGC 5694 (red circles) in the $[Na/Fe]$ – $[O/Fe]$ and $[Mg/Fe]$ – $[Al/Fe]$ planes, respectively. Five out of six stars have the same abundances of these elements, within the uncertainties. On the other hand, star #95 has O and Mg abundances consistent with the others, but it shows *significantly lower* Al and Na abundances.

As a sanity check, we analyzed also the Na resonance D doublet at 5890–5896 Å, a feature that is very strong even in our low-metallicity stars (~ 250 – 300 mÅ) and is not contaminated by interstellar Na lines, given the systemic velocity of the cluster. The abundance derived from these lines is very sensitive to temperature, gravity and EW uncertainty, with respect to the other Na lines used in this work. Still, it provides an independent test on the difference in Na abundance between star #95 and the other targets. The EWs have been obtained with the IRAF task *splot*, adopting a Voigt profile in order to properly take into account the contribution of the prominent wings. From NaD lines we confirm that the sodium abundance of star #95 is indeed significantly lower (by $\gtrsim 0.4$ dex) with respect to the other stars.

These findings provide a first indication that the self-enrichment processes that seem common to all massive GCs occurred also in NGC 5694. In light of the evidence collected for the Galactic GCs, we can consider star #95 as belonging to the first stellar generation of the cluster, while the

other five should belong to a subsequent generation, formed from the ejecta of the first stars. Although the sample is too small to draw any firm conclusion on this issue, the relative fraction of stars of the cluster labelled as second generation stars resembles that observed in Milky Way GCs, where the second generation stars currently account for $\sim 70\%$ of the total stellar content of the clusters (Carretta et al. 2009a).

Concerning the origin of NGC 5694, it is interesting to note that the stars considered in the present study lie at the margins of the $[Na/Fe]$ – $[O/Fe]$ and $[Mg/Fe]$ – $[Al/Fe]$ distribution of stars in classical GCs, and star #95 has $[Al/Fe]$ and, in particular, $[Na/Fe]$ ratios compatible with the stars from metal-rich Sgr clusters and Rup 106 (green asterisks in Fig. 6 and 7) that, in turn, are clearly different from genuine Galactic GCs also in this respect (i.e. they can be chemically tagged as extra-galactic also based on their abundances of Na, O, Mg, Al; see Bellazzini 2013).

5 A BRIEF CHEMICAL HISTORY OF NC5694

The chemical composition of NGC 5694 is remarkably different with respect to the Galactic stars of similar metallicity. In particular, NGC 5694 exhibits at least two main chemical peculiarities when it is compared with Milky Way (field/GC) stars:

- solar-scaled $[\alpha/Fe]$ ratios, with the only exception of $[Si/Fe]$ (that appears to be enhanced with respect to the solar value);
- deficiency of neutron-capture elements, both those usually associated to slow neutron-capture (as Y, La and Ba) and to rapid neutron-capture (Eu).

Since α -elements are produced mainly in the massive stars through hydrostatic (for O and Mg) and explosive (for Si, Ca, and Ti) nucleosynthesis by Type II SNe, while iron is produced also by Type Ia SNe, the $[\alpha/Fe]$ ratio is commonly adopted as tracer of the relative contribution of Type II and Ia SNe. In the Galactic Halo the $[\alpha/Fe]$ ratio remains nearly constant around $[\alpha/Fe] \simeq +0.3$ up to $[Fe/H] \sim -1.0$, where it begins to decline (the so-called *knee*), reaching $[\alpha/Fe] \sim 0.0$ at $[Fe/H] \sim 0.0$. Generally, the iron content of the *knee* marks the metallicity reached by the system when the ejecta of Type Ia SNe are well mixed in the interstellar medium and their chemical signatures dominate the gas, because the Type Ia SNe have longer timescales than Type II SNe. Systems characterized by star formation rates lower than that of the Milky Way will have the *knee* shifted toward lower metallicity, as observed in dSph galaxies (see Fig. 3 and Tolstoy et al. 2009, for a discussion and references). Thus, the low (solar) $[\alpha/Fe]$ abundance ratios (lower than those observed in the Galactic Halo stars of similar metallicity) clearly suggest that this cluster formed from a gas enriched by both Type II and Type Ia SNe and likely in an environment characterized by a star formation rate slower than that typical of the Galactic Halo.

The interpretation of the neutron-capture elements abundances is complicated by the multiplicity of their nucleosynthesis sites. Basically, the main contributors to slow neutron-capture elements (like Y, La and Ba) at the solar metallicity are the AGB stars with initial mass between ~ 1 and $\sim 4 M_{\odot}$ during the thermal pulses stage (see e.g.

Busso et al. 1999), the so-called main s-component. Slow neutron-capture processes occur also in massive ($M > 8M_{\odot}$) stars during the convective core He burning phase, the so-called weak s-component (see e.g. Raiteri et al 1991; Pignatari et al. 2010). These elements are not totally built from s-processes because a small fraction (of the order of $\sim 20\%$ for these elements) is produced from rapid neutron-captures. The efficiency of the r-process can be estimated from the analysis of Eu, considered a pure r-process element, being formed in the solar system almost totally from r-process nucleosynthesis ($\sim 97\%$, see e.g. Burris et al. 2000). The precise site of the r-process is still debated but it is usually associated to massive stars where a relevant neutron flux is available. The chemical abundances of neutron-capture elements in NGC 5694 are unusual for both field and GC stars in the Galactic Halo and clearly point out that NGC 5694 has formed from gas enriched in a different way with respect to the Halo.

In the Milky Way, no GCs with such a low [Ba/Fe] ratio is observed (see D’Orazi et al. 2010), while among field stars [Ba/Fe] decreases in the metal-poor regime, at $[\text{Fe}/\text{H}] < -2.5$ dex (Barklem et al. 2005). Also, NGC 5694 is remarkably deficient in Eu ($[\text{Eu}/\text{Fe}] < 0.0$), while the stars of similar metallicity observed in the Milky Way (as well as in the LMC and dSphs) are characterized by enhanced values of [Eu/Fe]. The Eu depletion seems to suggest that NGC 5694 formed from gas where the enrichment by r-process has been less efficient than in other galaxies of the Local Group studied so far. This finding could explain (at least partially) the low Y, Ba and La abundances. Because the contribution by AGB stars starts to be relevant after $\sim 100\text{--}300$ Myr from the first burst of star formation in the galaxy where the cluster formed, these elements are produced mainly from r-processes.

L06 include among the chemical peculiarities of NGC 5694 also the low [Cu/Fe] ratio. In light of our differential analysis with NGC 6397, that shows a [Cu/Fe] ratio higher than that of NGC 5694 by only 0.1 dex, we are cautious to over-interpret the Cu abundance in the cluster. The stars in the Milky Way show a relevant scatter of [Cu/Fe] in the metal-poor regime: the bulk of the stars around $[\text{Fe}/\text{H}] \sim -2$ dex has $[\text{Cu}/\text{Fe}] \sim -0.7$ dex, but both the sample of Mishenina et al. (2002) and Bihain et al. (2004) include stars with $[\text{Cu}/\text{Fe}] \sim -1$ dex at the metallicity of NGC 5694. On the other hand, the sample of GCs by Simmerer et al. (2003) shows higher (by about 0.3 dex) values of [Cu/Fe] for metal-poor clusters. Unfortunately, the dataset by Simmerer et al. (2003) does not include NGC 6397 and we cannot perform a direct comparison between the two analyses¹¹.

¹¹ Simmerer et al. (2003) derived the Cu abundance for the majority of their stars from the Cu line at 5782 \AA and only for a sub-sample of star they are able to measure the line at 5105 \AA , used in our work. In order to check for possible offset between the two transitions, we measured them in the solar flux spectrum of Neckel & Labs (1984), finding differences in the derived abundances less than 0.05 dex (and in excellent agreement with the solar Cu abundance). Also, we checked that there are no difference between the employed oscillator strengths, the hyperfine components and the isotopic ratio for the 5105 \AA between us and Simmerer et al. (2003).

6 WHO ARE THE RELATIVES OF NGC 5694?

Our chemical analysis confirms and extends the first findings by L06, definitely tagging NGC 5694 as a *foster son* of the Galactic Halo, therefore a cluster of extra-Galactic origin. Its abundance pattern is significantly different from the other Galactic GCs of similar metallicity, as well as from the bulk of metal-poor Halo field stars. The cluster most likely originated in a dwarf galaxy having a slower chemical evolution and a lower enrichment by the r-process with respect to the Milky Way (see Tolstoy et al. 2009).

NGC 5694 is, by far, the most metal-poor GC chemically tagged as an interloper of the Galactic halo. We note that clusters having similar metallicity, that are known to be members of the Sgr dSph (Ter 8, Arp 2, M 54) do not show the chemical anomalies that allowed L06 and us to recognize NGC 5694 as an incomer: they have α , Eu and Ba abundances fully compatible with the classical Halo population (see also Mottini & Wallerstein 2008). Hence, an association of NGC 5694 with the Sgr galaxy or with its tidal stream can be excluded on the basis of the chemical abundance pattern alone (thus confirming the conclusions by Law & Majewski 2010).

None of the dSphs studied so far fully matches the chemical composition of NGC 5694 at the same metallicity level, since, in particular, they display higher abundances of neutron-capture elements, on average. Indeed, the dSph stars with an iron content around $[\text{Fe}/\text{H}] \sim -2$ cover a large range of [Ba/Fe] values typically with $[\text{Ba}/\text{Fe}] > -0.5$ dex (but basically compatible with the Galactic stars), and *enhanced* [Eu/Fe] (see for instance Fig. 13 in Tolstoy et al. 2009). Still, the fraction of stars reaching $[\text{Eu}/\text{Fe}] \lesssim +0.2$ is larger among dSphs than among the Halo population, in the considered metallicity regime. Two Ba-poor stars have been identified in the Carina dSph by Lemasle et al. (2012, namely MKV0397) and Venn et al. (2012, namely #5070). MKV0397 has $[\text{Fe}/\text{H}]_{\text{I}} = -1.99$ and $[\text{Ba}/\text{Fe}]_{\text{II}} = -0.87$, but with $[\text{Ca}/\text{Fe}] = +0.39$ (unfortunately, the Eu abundance is not provided for this star). #5070 has $[\text{Fe}/\text{H}]_{\text{I}} = -2.15$ and $[\text{Ba}/\text{Fe}]_{\text{II}} = -1.12$, showing also solar abundances for [Ca/Fe] and [Ti/Fe] but a strong (-0.36) depletion for [Mg/Fe], while a slightly over-solar ($+0.13$) [Eu/Fe] ratio is found. A Bar-poor star has been found also in the Draco dSph by Cohen (2004, namely XI-2), having $[\text{Fe}/\text{H}]_{\text{I}} = -1.99$ and $[\text{Ba}/\text{Fe}]_{\text{II}} = -1.12$, but [Ca/Fe] and [Ti/Fe] are heavily depleted (< -0.3 dex). We conclude that the available data are not incompatible with the hypothesis that NGC 5694 was born in a system (chemically) similar to present-day dSphs, but the chemical properties of the cluster are pretty extreme with respect to the overall distribution of dSph stars.

Also Ultra Faint Dwarf galaxies (UFD) typically have stars as metal-poor as NGC 5694 with solar or sub-solar $[\alpha/\text{Fe}]$ ratios (Vargas et al. 2013). While abundance estimates for r-process elements are largely lacking for these systems, it is very intriguing to note that stars with $[\text{Fe}/\text{H}] \simeq -2.0$, $[\alpha/\text{Fe}] \simeq 0.0$ and $[\text{Ba}/\text{Fe}] \lesssim -0.5$, i.e. fully analogous to NGC 5694 stars, have been actually observed in some UFD (namely CVn II and Leo IV, see Francois et al. 2012).

In a similar way, we check also the possibility that NGC 5694 can be associated to the LMC. Johnson et al. (2006) and Mucciarelli et al. (2010) provide conflicting results about the $[\alpha/\text{Fe}]$ ratios in old LMC GCs. The clus-

ters analysed by Johnson et al. (2006) have solar-scaled $[\alpha/\text{Fe}]$, compatible with the dSph stars and with the abundances in NGC 5694. On the hand, the GCs discussed by Mucciarelli et al. (2010) have enhanced $[\alpha/\text{Fe}]$ ratios, compatible with those of the Halo stars. However, both the analyses point to solar or enhanced $[\text{Ba}/\text{Fe}]$ ratios and enhanced $[\text{Eu}/\text{Fe}]$ for the LMC GCs. Thus, the different abundances of the neutron-capture elements (and in particular the different level of enrichment by the r-process) do not support the idea that NGC 5694 formed in the LMC.

It is interesting to note that the chemical oddities that make NGC 5694 such a peculiar object are – to some extent – shared by Rup 106, a cluster whose extra-Galactic origin has been suspected since long time (Buonanno et al. 1990; Lin & Richer 1992; Fusi Pecci et al. 1995). As in NGC 5694, the two giant stars of Rup 106 discussed by Brown et al. (1997) have $[\alpha/\text{Fe}]$, $[\text{Ba}/\text{Fe}]$ and $[\text{Eu}/\text{Fe}]$ ratios lower than those of the Halo field stars of similar metallicity. The two clusters lie in the same broad region of the outer halo, having Galactic longitude, latitude and galactocentric distance $(l, b, R_{GC})_{\text{NGC 5694}} = (331.1^\circ, +30.4^\circ, 29.4 \text{ kpc})$ and $(l, b, R_{GC})_{\text{Rup106}} = (300.9^\circ, +11.7^\circ, 18.5 \text{ kpc})$, according to Harris (1996, 2010 edition). They also have very similar galactocentric radial velocity ($V_{GSR} = -233$ and -231 km/s , for Rup 106 and NGC 5694, respectively; Law & Majewski 2010). By taking into account its chemical composition, as derived in the present study, we confirm that NGC 5694 is as old as the oldest Galactic GC (in particular, as old or even slightly older than NGC 6397; De Angeli et al. 2005). This implies that Rup106 is a couple of Gyr younger than NGC 5694 (see Dotter et al. 2010, 2011). In turn, since Rup106 is also ~ 0.5 dex more metal-rich than NGC 5694, this may hint at a common age-metallicity relation, as observed in the GC systems of some dSphs (see, e.g. Montegriffo et al. 1998; Forbes & Bridges 2010). Given all the above considerations, the hypothesis of a common origin for the two clusters, in the same (now disrupted) dwarf satellite of the Milky Way, cannot be easily dismissed.

ACKNOWLEDGMENTS

The authors warmly thank the referee for his/her valuable comments and suggestions. M.B. acknowledges the financial support from PRIN MIUR, project: *The Chemical and Dynamical Evolution of the Milky Way and Local Group Galaxies*, prot. 2010LY5N2T. M.C. and P.A. are supported by the Chilean Ministry for the Economy, Development, and Tourism's Programa Iniciativa Científica Milenio through grant P07-021-F, awarded to The Milky Way Millennium Nucleus; by the BASAL Center for Astrophysics and Associated Technologies (PFB-06); by Proyecto Fondecyt Regular #1110326; and by Proyecto Anillo ACT-86. We thank E. Carretta for sharing with us the unpublished data for the Ti abundances in Galactic GCs.

REFERENCES

- Abadi, M.G., Navarro, J.F., Steinmetz, M., MNRAS, 365, 747
- Alonso, A., Arribas, S., & Martinez-Roger, C., 1999, A&AS, 140, 261
- Asplund, M., 2005, ARA&A, 43, 481
- Barklem, P. S., Piskunov, N., & O'Mara, B. J., 2000. A&AS, 142, 467
- Barklem P. S., Christlieb, N., Beers, T. C., Hill, V., Bessell, M. S., Holmberg, J., Marsteller, B., Rossi, S., Zickgraf, F.-J., & Reimers, D., 2005, A&A, 439, 129
- Bell, E.F., et al., 2008, ApJ, 680, 295
- Bellazzini, M., Ferraro, F.R., Ibata, R., 2003, AJ, 125, 188
- Bellazzini, M., 2013, in Origin and Complexity of Massive Star Clusters, XXVIIth IAU General Assembly SpS1, G. Piotto and E. Vesperini eds., Highlights in Astronomy, in press (arXiv:1210.6169)
- Bensby, T., Feltzing, S., Lundstrom, I., & Ilyin, I., 2005, A&A, 433, 185
- Bihain, G., Israelian, G., Rebolo, R., Bonifacio, P., & Molero, P., 2004, A&A, 423, 777
- Brown, J. A., Wallerstein, G., & Zucker, D., 1997, AH, 114, 180
- Brown, J. A., Wallerstein, G., & Gonzales, G., 1999, AJ, 118, 1245
- Bullock, J.S., Johnstone, K.V., 2005, ApJ, 635, 931
- Busso, M., Gallino, R., & Wasserburg, G. J., 1999, ARA&A, 37, 239
- Buonanno, R., Buscema, G., Fusi Pecci, F., Richer, H.B., Fahlman, G.G., 1990, AJ, 100, 1811
- Burris, D. L., Pilachowski, C. A., Armandroff, T. E., Sneider, C., Cowan, J.J., & Roe, H., 2000, ApJ, 544, 302
- Caffau, E., Ludwig, H.-G., Steffen, M., Ayres, T. R., Bonifacio, P., Cayrel, R., Freytag, B., & Plez, B., 2008, A&A, 488, 1031
- Carney, B. W., Wright, J. S., Sneider, C., Laird, J. B., Aguilar, L. A., & Lantham, D. W., 1997, AJ, 114, 363
- Carretta, E., et al., 2009a, A&A, 505, 117
- Carretta, E., Bragaglia, A., Gratton, R., & Lucatello, S., 2009b, A&A, 505, 139
- Carretta, E., Bragaglia, A., Gratton, R., D'Orazi, V., Lucatello, S., 2009c, A&A, 508, 695
- Carretta, E., Bragaglia, A., Gratton, R., Lucatello, S., Bellazzini, M., Catanzaro, G., Leone, F., Momany, Y., Piotto, G., & D'Orazi, V., 2010, A&A, 520, 95
- Castelli, F., Gratton, R. G., & Kurucz, R. L., 1997, A&A, 318, 841
- Castelli, F., 2005, MSAIS, 8, 44
- Cohen, J. G., 2004, AJ, 127, 1545
- Cohen, J. G., & Ramirez, J., 2005, AJ, 129, 303
- Cohen, J. G., & Huang, W., 2009, ApJ, 701, 1053
- Correnti, M., Bellazzini, M., Dalessandro, E., Mucciarelli, A., Monaco, L., & Catelan, M., 2011, MNRAS, 417, 2411
- De Angeli, F., Piotto, G., Cassisi, S., Busso, G., Recio-Blanco, A., Salaris, M., Aparicio, A., Rosenberg, A., 2005, AJ, 130, 116
- D'Orazi, V., Gratton, R., Lucatello, S., Carretta, E., Bragaglia, A., & Marino, A. F., 2010, ApJ, 719L, 213
- Dotter, A., et al., 2010, ApJ, 708, 698
- Dotter, A., Sarajedini, A., Anderson, J., 2011, ApJ, 738, 74

Table 1. Fundamental parameters for target stars.

ID	G95-ID	RA _{J2000} [deg]	Dec _{J2000} [deg]	B	V	RV [km/s]	T_{eff} [K]	logg	v_t [km/s]
37	62	219.8853105	-26.5527808	17.025	15.644	-138.6±0.3	4180	0.65	1.90
57	51	219.8833781	-26.5442684	17.180	15.924	-140.0±0.4	4324	0.86	1.80
68	110	219.9161622	-26.5452373	17.276	16.094	-138.5±0.3	4414	0.99	1.80
82	109	219.9107318	-26.5464133	17.416	16.292	-151.2±0.4	4488	1.11	1.80
95	28	219.8684541	-26.5313730	17.498	16.414	-137.0±0.4	4540	1.19	1.80
105	68	219.8854188	-26.5660950	17.560	16.518	-136.9±0.5	4596	1.26	1.60

Table 2. Atomic data and measured equivalent widths of the UVES targets. The complete table is available in the electronic form.

Star	λ (Å)	Ion	loggf	χ (eV)	EW (mÅ)	σ_{EW} (mÅ)
NGC 5694-37	4882.1	Fe I	-1.640	3.420	48.00	5.69
NGC 5694-37	4927.4	Fe I	-2.070	3.570	20.20	3.02
NGC 5694-37	4950.1	Fe I	-1.670	3.420	53.50	4.75
NGC 5694-37	4985.2	Fe I	-0.560	3.930	76.90	5.29
NGC 5694-37	5002.7	Fe I	-1.530	3.400	57.60	3.61
NGC 5694-37	5014.9	Fe I	-0.300	3.940	79.60	3.17
NGC 5694-37	5028.1	Fe I	-1.120	3.570	79.20	5.20
NGC 5694-37	5044.2	Fe I	-2.020	2.850	60.70	4.70
NGC 5694-37	5090.7	Fe I	-0.440	4.260	60.10	3.74

- Edvardsson, B., Andersen, J., Gustafsson, B., Lambert, L., Nissen, P. E., & Tomkin, J., 1993, *A&A*, 275, 101
- Fellhauer, M., et al., 2007, *MNRAS*, 375, 1171
- Forbes, D., Bridges, T., 2010, *MNRAS*, 404, 1203
- Francois, P., et al., 2012, in *Origin of matter and evolution of galaxies*, AIP Conf. proceedings, 1484, 460
- Frebel, A., Simon, J. D., Geha, M., & Willman, B., 2010, *ApJ*, 708, 560
- Freeman, K. & Bland-Hawthorn, J., 2002, *ARA&A*, 40, 487
- Fulbright, J. P., 2000, *AJ*, 120, 1841
- Fusi Pecci, F., Bellazzini, M., Cacciari, C., Ferraro, F.R., 1995, *AJ*, 110, 1664
- Geisler, D., Piatti, A. E., Claria, J. J., & Minniti, D., 1995, *AJ*, 109, 605
- Gratton, R. G., Carretta, E., Claudi, R., Lucatello, S., & Barbieri, M., 2003, *A&A*, 404, 187
- Gratton, R. G., Carretta, E., & Bragaglia, A., *A&AR*, 20, 50
- Grevesse, N., & Sauval, A. J., 1998, *SSRv*, 85, 161
- Harris, W.E., Hesser, J.E., 1976, *PASP*, 88, 377
- Harris, W.E., 1996, *AJ*, 112, 1487
- Ibata, R.A., Martin, N.F., Irwin, M., Chapman, S., Ferguson, A.M.N., Lewis, G.F., McConnachie, A.W., 2007, *ApJ*, 671, 1591
- Ivans, I. I., Kraft, R. P., Kraft, R. P., Suntzeff, N. B., Smith, V. V., 1999, *AJ*, 118, 1273
- Ivans, I., I., Kraft, R. P., Sneden, C., Smith, G. H., Rich, R. M., & Shetrone, M., 2001, *AJ*, 122, 1438
- James, G., Francois, P., Bonifacio, P., Carretta, E., Gratton, R., & Spite, F., 2004, *A&A*, 427, 825
- Johnson, J. A., Ivans, I. I., & Stetson, P. B., 2006, *ApH*, 640, 801
- Koch, A., Grebel, E. K., Gilmore, G. F., Wyse, R. F. G., Kleyana, J. T., Harbeck, D. R., Wilkinson, M. I., & Wyn Evans, N., 2008, *AJ*, 135, 1580
- Koch, A. & McWilliam, A., 2011, *AJ*, 142, 63
- Law, D.R., Majewski, S.R., 2010, *ApJ*, 718, 1128
- Lawler, J. E., Wickliffe, M. E., den Hartog, E. A., & Sneden, C., 2001, *ApJ*, 563, 1076
- Lawler, J. E., Bonvallet, G., & Sneden, C., 2001, *ApJ*, 556, 452
- Lee, J.-W., & Carney, B. W., 2002, *AJ*, 124, 1511
- Lee, J.-W., López-Morales, M., & Carney, B. W., 2006, *ApJ*, 646, L119 (L06)
- Lemasle, B., Hill, V., Tolstoy, E., Venn, K. A., Shetrone, M. D., Irwin, M. J., de Boer, T. J. L., Starkenburg, E., & Salvadori, S., 2012, *A&A*, 538, 100
- Letarte, B., et al., 2010, *A&A*, 523, 17
- Lin, D.N.C., Richer, H.B., 1992, 288, L57
- Lind, K., Asplund, M., Barklem, P. S., & Belyaev, A. K., 2011, *A&A*, 528, 103L
- Lind, K., Charbonnel, C., Decressin, T., Primas, F., Grundahl, F., & Asplund, M., 2011, *A&A*, 527, 148
- Lovisi, L., Mucciarelli, A., Lanzoni, B., Ferraro, F. R., Gratton, R., Dalessandro, E., & Contreras Ramos, R., 2012, *ApJ*, 754, 91
- Lupton, R., 1993, in *Statistics in Theory and Practice* (Princeton, NJ: Princeton, Univ. Press)
- Mackey, A.D., et al., 2010, *ApJ*, 717, L11
- Mackey, A.D., et al., 2013, *MNRAS*, 429, 281
- McCall, M. L., 2004, *AJ*, 128, 2144
- McWilliam, A., Preston, G. W., Sneden, C., & Searle, L., 1995, *AJ*, 109, 2757
- Montegriffo, P., Bellazzini, M., Ferraro, F.R., Martins, D., Sarajedini, A., Fusi Pecci, F., 1998, *MNRAS*, 294, 315
- Mishenina, T. V., Kovtyukh, V. V., Soubrian, C., Travaglio, C., & Busso, M., 2002, *A&A*, 396, 189
- Mitshang, A.W., G. De Silva, S. Sharma, Zucker, D.B.,

Table 3. Abundance ratios for individual target stars.

ID	[Fe/H] I	[Fe/H] II	[O/Fe]	[Na/Fe]	[Mg/Fe]
Sun	7.50	7.50	8.76	6.33	7.58
37	-2.01±0.07	-1.83±0.06	0.01±0.11 (0.09)	0.18±0.06 (0.08)	0.12±0.04 (0.06)
57	-1.99±0.10	-1.89±0.05	0.00±0.11 (0.08)	0.10±0.05 (0.06)	0.14±0.04 (0.07)
68	-1.92±0.09	-1.83±0.04	-0.18±0.13 (0.08)	0.06±0.07 (0.07)	0.01±0.05 (0.07)
82	-1.94±0.09	-1.78±0.05	-0.04±0.11 (0.10)	0.08±0.06 (0.06)	0.06±0.06 (0.07)
95	-2.06±0.09	-1.85±0.04	0.13±0.12 (0.10)	<-0.30	0.15±0.06 (0.07)
105	-1.88±0.09	-1.81±0.04	0.03±0.14 (0.10)	0.07±0.07 (0.07)	0.05±0.07 (0.07)
ID	[Al/Fe]	[Si/Fe]	[Sc/Fe] II	[Ca/Fe]	[Ti/Fe] I
Sun	6.47	7.55	3.17	6.36	5.02
37	0.86±0.07 (0.07)	0.36±0.07 (0.03)	-0.24±0.10 (0.07)	0.03±0.02 (0.08)	0.01±0.06 (0.11)
57	0.92±0.06 (0.06)	0.35±0.09 (0.06)	-0.24±0.11 (0.07)	0.05±0.02 (0.08)	0.01±0.05 (0.13)
68	0.92±0.06 (0.06)	0.21±0.07 (0.04)	-0.31±0.10 (0.07)	0.00±0.02 (0.07)	0.05±0.05 (0.13)
82	0.86±0.11 (0.10)	0.25±0.12 (0.11)	-0.30±0.11 (0.08)	0.02±0.03 (0.07)	0.10±0.05 (0.12)
95	<0.60	0.35±0.08 (0.07)	-0.31±0.11 (0.07)	0.08±0.03 (0.07)	0.14±0.06 (0.12)
105	0.95±0.09 (0.08)	0.30±0.09 (0.07)	-0.35±0.10 (0.06)	0.01±0.04 (0.07)	0.10±0.10 (0.14)
ID	[Ti/Fe] II	[V/Fe]	[Cr/Fe]	[Mn/Fe]	[Co/Fe]
Sun	5.02	4.00	5.39	4.92	6.25
37	-0.19±0.05 (0.05)	-0.45±0.07 (0.13)	-0.14±0.05 (0.11)	-0.60±0.17 (0.14)	-0.16±0.13 (0.08)
57	0.00±0.09 (0.09)	-0.40±0.08 (0.13)	-0.17±0.06 (0.14)	-0.53±0.18 (0.16)	-0.16±0.22 (0.20)
68	-0.14±0.05 (0.06)	-0.29±0.06 (0.13)	-0.12±0.04 (0.13)	-0.41±0.17 (0.14)	-0.28±0.18 (0.15)
82	-0.13±0.07 (0.08)	-0.34±0.10 (0.15)	0.00±0.03 (0.11)	-0.61±0.26 (0.24)	-0.11±0.16 (0.12)
95	-0.04±0.08 (0.08)	-0.35±0.12 (0.16)	-0.16±0.05 (0.12)	-0.48±0.18 (0.15)	-0.31±0.18 (0.16)
105	-0.07±0.10 (0.11)	-0.30±0.12 (0.16)	-0.13±0.08 (0.13)	-0.31±0.17 (0.14)	-0.12±0.20 (0.17)
ID	[Ni/Fe]	[Cu/Fe]	[Y/Fe] II	[Ba/Fe] II	[La/Fe] II
Sun	6.25	4.21	2.24	2.13	1.17
37	-0.03±0.03 (0.08)	-0.99±0.14 (0.09)	-0.64±0.12 (0.12)	-0.76±0.16 (0.14)	<-0.25
57	-0.10±0.03 (0.10)	-1.03±0.15 (0.10)	-0.74±0.06 (0.05)	-0.62±0.18 (0.16)	<-0.20
68	-0.08±0.04 (0.10)	-0.89±0.15 (0.10)	-0.82±0.06 (0.06)	-0.69±0.16 (0.14)	<-0.20
82	-0.05±0.04 (0.10)	-0.88±0.15 (0.11)	-0.80±0.09 (0.09)	-0.73±0.16 (0.15)	<-0.20
95	0.02±0.04 (0.10)	-1.29±0.17 (0.13)	-0.75±0.06 (0.06)	-0.68±0.20 (0.18)	<-0.10
105	-0.13±0.06 (0.10)	-1.28±0.20 (0.17)	-0.73±0.11 (0.11)	-0.76±0.17 (0.15)	<0.00
ID	[Eu/Fe] II				
Sun	0.51				
37	<0.00				
57	<0.00				
68	<0.10				
82	<0.10				
95	<0.10				
105	<0.15				

2013, MNRAS, 428, 2321

Mottini, M., Wallerstein, G., & McWilliam, A., 2008, AJ, 136, 614

Mottini, M., Wallerstein, G., 2008, AJ, 136, 731

Mucciarelli, A., Origlia, L., & Ferraro, F. R., 2010, ApJ, 717, 277

Mucciarelli, A., Salaris, M., & Bonifacio, P., 2012, MNRAS, 419, 2195

Mucciarelli, A., Bellazzini, M., Ibata, R., Merle, T., Chapman, S. C., Dalessandro, E., & Sollima, A., 2012, MNRAS, 426, 2889

Mucciarelli, A., Pancino, E., Lovisi, L., Ferraro, F. R., & Lapenna, E., 2013, ApJ, 766, 78

Neckel, H., & Labs, D., 1984, SoPh, 90, 205

Newberg, H.J., Willet, B.A., Yanny, B., Xu, Y., 2010, ApJ, 711, 32

Osterbrock, D. E., Fulbright, J. P., Martel, A. R., Keane, M. J., Trager, S. C., & Basri, G., 1996, PASP, 108, 277

Pietrinferni, A., Cassisi, S., Salaris, M. & Castelli, F., 2004, ApJ, 612, 168

Piotto, G., et al., 2002, A&A, 391, 945

Pignatari, M., Gallino, R., Heil, M., Wiescher, M., Kappler, F., Herwig, F., & Bisterzo, S., 2010, ApJ, 710, 1557

Raiteri, C. M., Busso, M., Picchio, G., & Gallino, R., 1991, ApJ, 371, 665

Ramirez, S. V., & Cohen, J., 2002, AJ, 123, 3277

Table 4. Mean elemental abundances and intrinsic spreads for NGC 5694 and NGC 6397. The last column lists the difference δ between the mean abundances of NGC 5694 and NGC 6397. Only the elements that not show intrinsic spreads are listed.

Abundance ratio	NGC 5694		NGC 6397		δ
	mean \pm error	$\sigma_{int}\pm$ error	mean \pm error	$\sigma_{int}\pm$ error	
[Fe/H]	-1.98 \pm 0.03	0.00 \pm 0.04	-2.00 \pm 0.02	0.00 \pm 0.02	+0.02
[Fe/H]II	-1.83 \pm 0.01	0.00 \pm 0.02	-1.90 \pm 0.01	0.00 \pm 0.02	+0.07
[O/Fe]	-0.02 \pm 0.05	0.00 \pm 0.05	—	—	—
[Mg/Fe]	+0.10 \pm 0.02	0.00 \pm 0.06	—	—	—
[Si/Fe]	+0.30 \pm 0.03	0.00 \pm 0.05	+0.43 \pm 0.01	0.00 \pm 0.06	-0.13
[Ca/Fe]	+0.04 \pm 0.01	0.00 \pm 0.01	+0.37 \pm 0.01	0.00 \pm 0.01	-0.33
[Sc/Fe]II	-0.29 \pm 0.04	0.00 \pm 0.04	-0.05 \pm 0.02	0.00 \pm 0.04	-0.24
[Ti/Fe]	+0.05 \pm 0.02	0.00 \pm 0.04	+0.27 \pm 0.01	0.00 \pm 0.03	-0.22
[Ti/Fe]II	-0.13 \pm 0.02	0.00 \pm 0.04	+0.21 \pm 0.01	0.02 \pm 0.03	-0.34
[V/Fe]	-0.35 \pm 0.03	0.00 \pm 0.09	-0.14 \pm 0.03	0.00 \pm 0.04	-0.21
[Cr/Fe]	-0.14 \pm 0.02	0.00 \pm 0.02	-0.16 \pm 0.01	0.00 \pm 0.03	+0.02
[Mn/Fe]	-0.48 \pm 0.07	0.00 \pm 0.09	-0.55 \pm 0.04	0.00 \pm 0.06	+0.07
[Co/Fe]	-0.19 \pm 0.06	0.00 \pm 0.07	0.07 \pm 0.04	0.00 \pm 0.05	-0.26
[Ni/Fe]	-0.06 \pm 0.01	0.02 \pm 0.02	0.00 \pm 0.01	0.00 \pm 0.01	-0.06
[Cu/Fe]	-0.99 \pm 0.06	0.00 \pm 0.09	-0.89 \pm 0.04	0.00 \pm 0.10	-0.10
[Y/Fe]II	-0.77 \pm 0.03	0.00 \pm 0.03	-0.35 \pm 0.01	0.00 \pm 0.03	-0.42
[Ba/Fe]II	-0.71 \pm 0.06	0.00 \pm 0.06	0.12 \pm 0.02	0.00 \pm 0.03	-0.83
[La/Fe]II	<-0.25	—	0.24 \pm 0.02	0.00 \pm 0.04	—
[Eu/Fe]II	<0.00	—	0.44 \pm 0.01	0.00 \pm 0.03	—

Reddy, B. E., Tomkin, J., Lambert, D. L., & Allende Prieto, C., 2003, MNRAS, 340, 304

Reddy, B. E., Lambert, D. L., & Allende Prieto, C., 2006, MNRAS, 367, 1329

Rodrigues de Andrade, L., Catelan, M., & Smith, H.A., 2012, IBVS, 6037, 1

Sbordone, L., Bonifacio, P., Buonanno, R., Marconi, G., Monaco, L., & Zaggia, S., 2007, A&A, 465, 815

Schlaufman, K.C., Rockosi, C.M., Lee, Y.S., Beers, T.C., Allende Prieto, C., Rashkov, V., Madau, P., Bizyaev, D., 2012, ApJ, 749, 77

Shetrone, M., Côté, P., & Sargent, W. L. W., 2001, ApJ, 548, 592

Shetrone, M., Venn, K. A., Tolstoy, E., Primas, F., Hill, V., & Kaufer, A., 2003, AJ, 125, 684

Simmerer, J., Sneden, C., Ivans, I. I., Kraft, R. P., Shetrone, M. D., & Smith, V. V., 2003, AJ, 125, 2018

Sneden, C., McWilliam, A., Preston, G. W., Cowan, J. J., Burris, D. L., & Armosky, B. J., 1996, ApJ, 467, 840

Sneden, C., Kraft, R. P., Shetrone, M. D., Smith, G. H., Langer, G. E., & Prosser, C. F., 1997, AJ, 114, 1964

Sneden, C., Kraft, R. P., Guhatahkurta, P., Peterson, R. C., & Fulbright, J. P., 2004, AJ, 127, 2162

Stephens, A., & Boesgaard, A. M., 2002, AJ, 123, 1647

Stetson, P. & Pancino, E., 2008, PASP, 120, 1332

Tolstoy, E., Hill, V. & Tosi, M., 2009, ARA&A, 47, 371

Valcarce, A. A. R., & Catelan, M., 2008, A&A, 487, 185

Valcarce, A. A. R., & Catelan, M., 2011, A&A, 533, 120

Vargas, L.C., Geha, M., Kirby, E.N., Simon, J.D., 2013, ApJ, 767, 134

Venn, K. A., et al., 2012, ApJ, 751, 102